Lawrence Berkeley Laboratory
UNIVERSITY OF CALIFORNIA

Materials & Chemical Sciences Division

National Center for Electron Microscopy

Invited Keynote Address presented at the Fifth International Conference on Ferrites, Bombay, India, January 9–14, 1989, and to be published in the Proceedings

High Resolution Electron Microscopy and Microanalysis of Ferrites and Cuprates

G. Thomas

November 1988

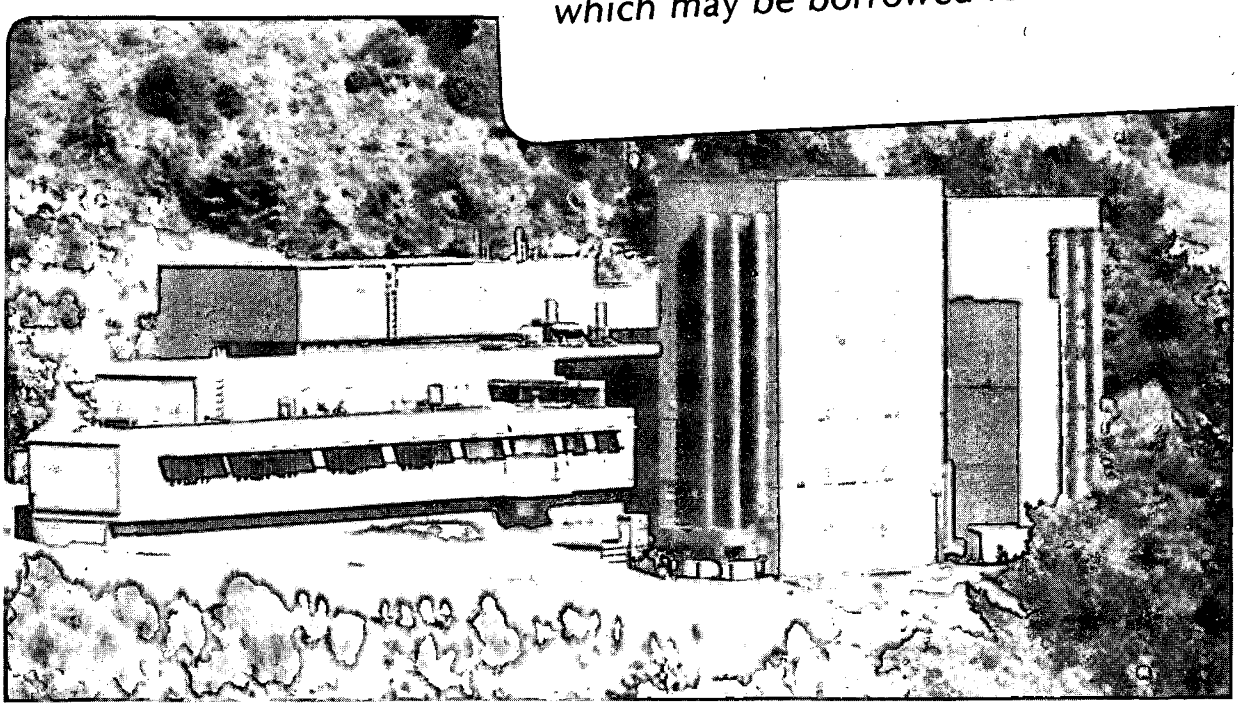

Prepared for the U.S. Department of Energy under Contract Number DE-AC03-76SF00098.

HIGH RESOLUTION ELECTRON MICROSCOPY AND MICROANALYSIS OF FERRITES AND CUPRATES

GARETH THOMAS, PROFESSOR, MATERIALS SCIENCE, UNIVERSITY OF CALIFORNIA, BERKELEY CA, AND SCIENTIFIC DIRECTOR, NATIONAL CENTER FOR ELECTRON MICROSCOPY, LAWRENCE BERKELEY LABORATORY, MATERIALS AND CHEMICAL SCIENCES DIVISION, 1 CYCLOTRON, BERKELEY, CA 94720.

1. INTRODUCTION-Although ferrites and cuprates are produced for quite different properties and applications - the former mainly for magnetic recording and the latter for potential high temperature superconducting applications, both classes of materials are ceramics. Ceramics in general have similar problems in processing to achieve the desired purity of composition, microstructures, morphology and properties, and hence the inter-relationships between these factors are of great concern for materials scientists and engineers. For example, defects such as intergranular phases are common to many ceramic systems, as illustrated in fig. 1. Thus the characterization of ceramics at the highest levels of spatial and spectroscopic resolutions are of supreme importance. It is in this regard that a modern transmission electron microscope (TEM), such as the unique 1.6A^{o} atomic resolution microscope (ARM) at Berkeley, is so valuable because so much information is obtainable in one instrument (1) as demonstrated in fig. 2. Unfortunately, except in a few rare cases, the characterization of magnetic structures in conventional transmission electron microscopes using Lorentz Imaging of

domains or domain walls must be done at low resolution, i.e., by using very weak or zero objective lens currents (and hence high spherical aberration) in order to avoid saturation of the specimen by the objective lens field (1). Although a special field free objective lens has been designed for magnetic imaging at better than $20A^o$ resolution (2) this is not yet widely available and not in conjunction with instruments equipped with field emission guns at higher than 200 kV which are required to obtain adequate intensities for differential phase contrast imaging (3). The basic aspects of electron microscopy can be found in the literature e.g., ref. (1) and in refs. 4,5 for high resolution image interpretation. An important method for atomic (site occupancy analysis is described in ref. (6).

2. Ferrites-For the purposes of illustration examples will be drawn from our research on soft ferrites for magnetic recording which have notable advantages of good resistivity in the insulating range, attractive magnetic properties at high frequencies and good corrosion resistance. For recording heads, low coercivities and high initial permeabilities (μ') are required. Mn-Zn ferrites are usable without serious losses up to 500 although drops rapidly (fig. 3). To reduce eddy current losses at high frequencies, doping (e.g. with CaO) is sometimes used, but as described by Lin et al. (7) this often results in undesirable grain boundary phases such as Ca-Si containing glasses which pin domain walls and hence reduce permeability. An example of such pinning is shown in fig. 4. Thus, the attainment of high purity and large grain sizes is necessary so as to improve these ferrites. The need for better materials for high frequency recording lead to the development of soft hexagonal barium ferrites (8) called "Ferroxplana"

of which the Y-type (9) hexagonal $Ba_2Me_2Fe_{12}O_{22}$ ceramics are very promising (fig. 3). In current work (10,11) such ferrites of specific composition $Ba_2Cu_{0.8}Zn_{1.2}Fe_{12}O_{22}$ have been prepared by co-precipitation (12). Zn is partially replaced by Cu to increase magnetic saturation. Figure 5 shows the magnetic properties of such materials in different forms. Figure 6 shows that well oriented polycrystals can be prepared. However, even the oriented polycrystals (fig. 6) are not single phase as shown in figs. 7,8. Magnetic domains have not been resolved indicating they are single domain particles. These intra and intergranular phases have the compositions listed below, (Table 1 a-c) using a 200 A° probe size.

Table 1 EDX Analysis

(a)

Inter-granular particle	Fe	Cu	Zn	Ba
Atomic %	65.37 ± 0.51	13.99 ± 0.26	19.18 ± 0.34	0.72 ± 0.17

(b)

Cu TGJ	Fe	Cu	Zn	Ba
Atomic %	4.84 ± 0.16	93.68 ± 0.74	0.69 ± 0.12	0.79 ± 0.21

(c)

Ba TGJ	Fe	Cu	Zn	Ba	Si
Atomic %	7.37 ± 0.36	2.63 ± 0.35	0.63 ± 0.26	59.74 ± 1.54	29.63 ± 0.40

3. SUPERCONDUCTING "HIGH T_C CUPRATES"-The recent discovery of superconductivity above 100K in Bi-Ca-Sr-Cu-O has further fueled the excitement prevailing in this area of research since the discovery of "warm" ceramic superconductors such as Y-Ba-Cu-O (13). The superconducting phase in this system, described by the general composition of $Bi_2Sr_2Cu_nCa_{n-1}O_y$, (with n=1,2,3,and sometimes 4) exhibits polytypoid-like behavior (14). The T_c is known to increase with "n", the number of Cu-O layers. The stacking sequence in these complex oxides has been revealed by atomic resolution imaging (15), and is similar to other well-known oxide ceramics, e.g.refs. 16,17. In fig. 9 (a), a [110] ARM image of the n=3 (T_c=110K) polytypoid is shown. Since the projection of the atomic potential is imaged, images of the Bi atoms (Z=83) are the largest, while those of Ca are the smallest. Thus, replacement of Ca by Bi (their ionic radii are almost the same) can be directly identified. The SEMPER processed image in fig. 9b shows another interesting detail of the structure. The contrast corresponding to the central Cu-O layer (indicated by arrows) is quite different from that of the other two rows, suggesting a deficiency of oxygen along that "chain". Image simulations confirm this inference. In figs. 10 (a&b) the [110] projected potential and a series of simulated images are shown respectively for the perfect crystal. In figs. 10 (c&d) the same are shown for a crystal in which the oxygen atoms from the central Cu-O row are removed. In the simulated image in (d), the contrast of the central Cu-O row is different from that of the other two rows, as seen in the processed image in fig. 9 (b). High resolution imaging, in conjunction

with EDX microanalysis, has also shown that the grain boundaries are Cu and Ca deficient, thus causing the lower T_c n=1 or 2 polytypoids to form there. Figure 11 (a) is a lattice fringe image showing the polytypoid structures adjacent to the grain boundary. The T_c values decrease towards the grain boundary due to the change in the composition and T_c for each polytypoid. Figure 11 (b) is a typical lattice fringe image of a sample with PbO added, showing a uniform n=3 structure up to the grain boundary. The resistivity plot of the leaded samples are quite different from those of the unleaded samples (14). As shown in fig. 13 current work suggests that controlled additions of PbO enables liquid phases rich in Pb to form intergranularly and removes the low T_c phases adjacent to boundaries. This is the likely reason for the disappearance of the step in the resistivity. Similar effects have been observed in SiAlONs, fig. 12, in which the cation:anion ratio changes close to the grain boundary, causing the formation of different polytypes (16,17). It is very likely that the low T_c polytypoids adjacent to the grain boundaries can affect intergranular "connectivity" (18).

In the case of Y-Ba-Cu-O, high resolution imaging of the grain boundaries has shown that approximately 70% of the grain boundaries planes are of the (001) type. Figure 14 (a) shows one such typical grain boundary, in which the upper grain is in the [100] zone and the lower in the [441] zone (19). Figure 14 (b) shows a SEMPER processed image in which only the upper grain has been processed. The interesting feature in this image is that the grain boundary plane is a BaO plane. It is well known that BaO is an insulator, and hence is likely to be a barrier to the movement of the super-current from one grain to another. In the case of the BCSCO ceramics, the grain boundary plane is generally a Bi-O plane. If this is generally true, then it will be difficult to improve J_c by grain boundary engineering. In addition to these polytypoids, the alkaline earth cuprates are complicated due to other modulations including incommensurate structures along the b-c plane and a new b axis modulated structure has recently been observed in our laboratory.

It is concluded that compositional and structural defects near grain boundaries are responsible for the low critical currents in polycrystals and more emphasis should be placed on studies of phase equilibria in these multicomponent oxide superconductors.

SUMMARY-High resolution electron microscopy and microanalysis are very important to the characterization and understanding of magnetic and conducting ceramics. Grain boundary problems are generic. They can be avoided by developing oriented single crystals, and possibly by properly oriented polycrystals of uniform desired compositions and structure. This is the research realm to which which materials scientists and engineers should pay special attention.

ACKNOWLEGEMENT-This work was supported by the Director, Office of Basic Energy Research, Office of Basic Energy Sciences, Materials Science Division of the U.S. Department of Energy under Contract No. DE-CO3-76SF00098. I wish to acknowledge the considerable contributions of Dr. R. Ramesh (now at Belcor, N.J.) and Dr. C. Hetherington, and all of the staff at NCEM and to Ms. Thantu Huynh for the results on Y-Ba ferrites.

REFERENCES

1. Thomas, G. and M.J. Goringe. Transmission Electron Microscopy of Materials, J. Wiley & Sons, NY 1979.
2. Tsuno, K. and Inone, M. Optik 67 No. 4: 363, 1986.
3. Chapman, J.N. and Morrison, G.R. J. Mag. & Magn. Mats. 35:254 1983.
4. Kilaas, R. in Proc. 45th Ann. Mtg. EMSA: 66-69. 1987.
5. O'Keefe, M.A. and Kilaas, R. in Proc. 6th Pfefferkorn Conf. 1988.
6. Krishnan, K.M., Rez, P. and Thomas, G. Acta Cryst. B41: 396, 1985.
7. Lin, I.Nan, Mishra, R.K. and Thomas, G. IEEE Trans. on Mag. 20 (1): 134, 1984.
8. Jonker, G.H., Wijn, H.P.J. and Braun, P.B. Phillips Tech. Rev. 18, 145, 1956/57.
9. Smit, J. & Wijn, H.P.J.Ferrites, Phillips Tech. Lib.(Eindhoven) 1959.
10. Huynh, T. M.S. Thesis, U.C. Berkeley 9/88; LBL-25968.
11. Ramesh, R. U.C. Berkeley - unpublished.
12. Thanks to B. West and D.Yang for supplying samples and magnetic data.
13. Bednorz, J.G. and Muller, K.A. Z. Phys. B64 189, 1986.
14. Ramesh, R., Thomas, G., Green, S.M., Jiang, C., Mei, Y., Rudee, M.L and Luo, H.L., Phys. Rev. 38 7070, 1988.
15. Hetherington, C.J.D., Ramesh, R., O'Keefe, M.A., Kilaas, R., Thomas, G., Green, S.M., and Luo, H.L. Appl. Phys. Lett. 53: 1016, 1988.
16. Clarke, D.R. J. Amer. Cer. Soc. 63: 208, 1980.
17. van Tendeloo, G., Faber, K.T. and Thomas, G., J. Materials Sci. 18:525,1983.
18. Ramesh, R., Thomas, G., Green, S.M., Jiang, C., Mei, Y. and Luo, H.L. Luo, Proc. 1988 Applied Superconductivity Conf. S.F. 1988.
19. Zandbergen, H.W., Gronsky, R. and Thomas, G., J. de Microcopie et

du Spectroscopie Electronique, 1988, in press.

FIGURE CAPTIONS

Fig. 1 Some generic microstructures in ceramics: polycrystals contain intergranular phases (glassy-crystalline) which affect many properties. Also, misorientations reduce connectivity at boundaries and intragranular defects and polytypes also affect properties.

Fig. 2 Characterization by transmission electron microscopy.

Fig. 3 Frequency dispersion curves for Mn-Zn ferrite and "ferroxplana."

Fig. 4 Lorentz imaging showing domain walls moving under an applied field to become pinned at grain boundary in CaO doped Mn-Zn ferrite (ref. 7). The boundary contains an amorphous Ca-Si rich phase not resolved in this imaging mode.

Fig. 5 Hysteresis curves for non and oriented polycrystalline Y-(BaCuZn) ferrite and for single crystalline Y-Zn_2 sample (ref. 12).

Fig. 6 Conventional TEM images of Y(CuZn) sample (a) with c-axis in plane and (b) with the c-axis perpendicular to the sample surface.

Fig. 7 High resolution lattice image showing two phases at a triple grain junction (see Table 1b,c).

Fig. 8 Intragranular particle and CBD pattern showing its 3-fold cubic symmetry. EDX analysis shows particles to be Ba deficient (Table 1a).

Fig. 9 (a) ARM image of the n=3 [T_c=110K] polytypoid in the Bi-Ca-Sr-Cu-O system; (b) image in (a) after SEMPER processing. Note the intensity difference in the central Cu-O row compared to the other rows. (Courtesy Appl. Phys. Lett.)

Fig 10 (a) [110] projected potential for perfect n=3 structure; (b) simulated images corresponding to (a); (c) projected potential for a structure where the oxygen from the central Cu-O row has been removed; (d) simulated images corresponding to the structure in (c) showing the intensity difference between central Cu-O row and other two rows. (Courtesy Appl. Phys. Lett.)

FIGURE CAPTIONS

Fig. 11 Lattice fringe image near grain boundary of un-leaded sample showing change in composition (and reduction in T_c from 110°K to 10°K) from that of n=3 to n=1; (b) lattice fringe in leaded sample showing uniform composition of n=3 up to grain boundary. (Courtesy Phys. Rev. B.)

Fig. 12 Comparison of polytypoids in Sialons with Bi/Pb cuprates. Phase diagrams (top R), known for Sialons, are not yet known for the superconductors.

Fig. 13 A plot of resistivity vs. temperature. +,---: $Bi_2Sr_2Ca_2Cu_4O_y$, 870-875°C, 72h; o,—: $Bi_{1.4}Pb_{0.6}Sr_2Ca_2Cu_3O_y$, 860-865°C, 60h.

Fig. 14 (a) HREM image: grain boundary in Y-Ba-Cu-O ceramic; (b) SEMPER processed image in which upper grain in [100] axis has been processed to reveal the grain boundary plane to be a Ba-O plane (ref. 19).

Some Generic Microstructures: Ceramics

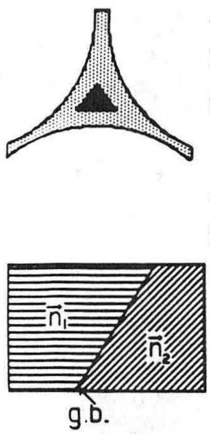

Grain boundaries / interfaces	Examples	Properties limited
Amorphous films	Si_3N_4	Creep
Partly crystalline films	Some Sialons	Creep
	Ferrites	Permeability
	Varistors	Voltage drop required
Additives / impurities	ß Na alumina	Na^+ conduction
	$YBa_2Cu_3O_{7-x}$	Conduction a-b plane
	$Bi_2Sr_2Cu_nCa_{n-1}O_y$ polytypoids of low T_c	Affects T_c and J_c
	ZrO_2 / mullite composites	Varied (creep, etc.)

XBL 8712-5343A

Fig. 1

CHARACTERIZATION BY ELECTRON MICROSCOPY

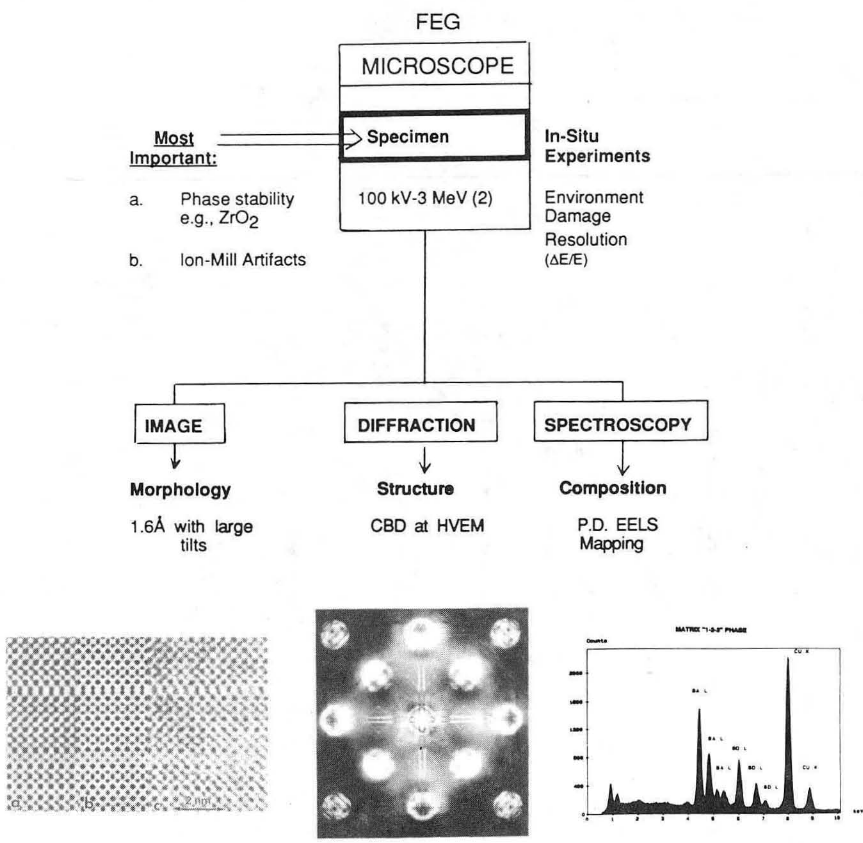

XBB 882-1149

Fig.2

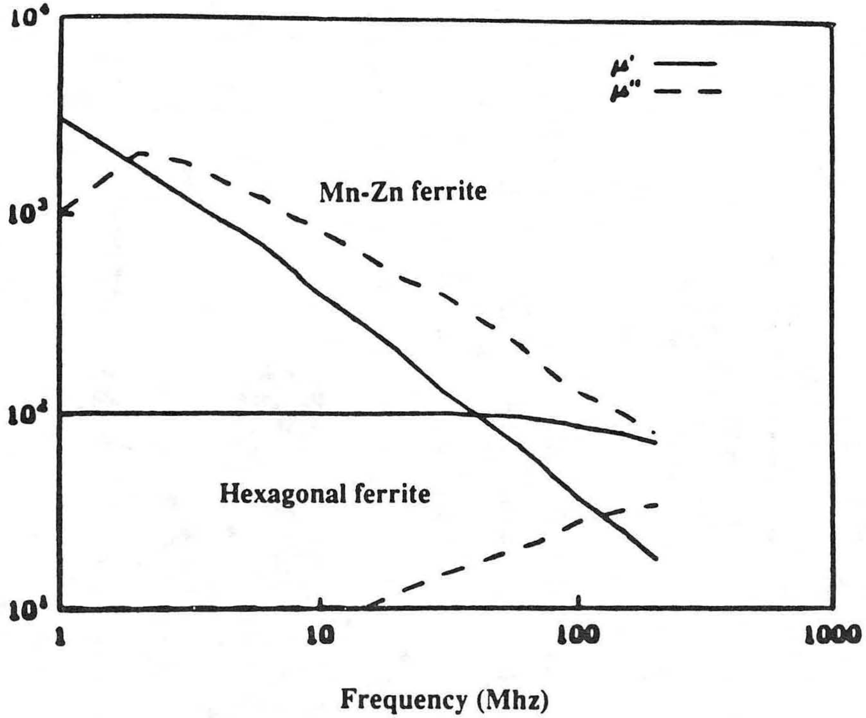

XBL 888-2716

Fig. 3

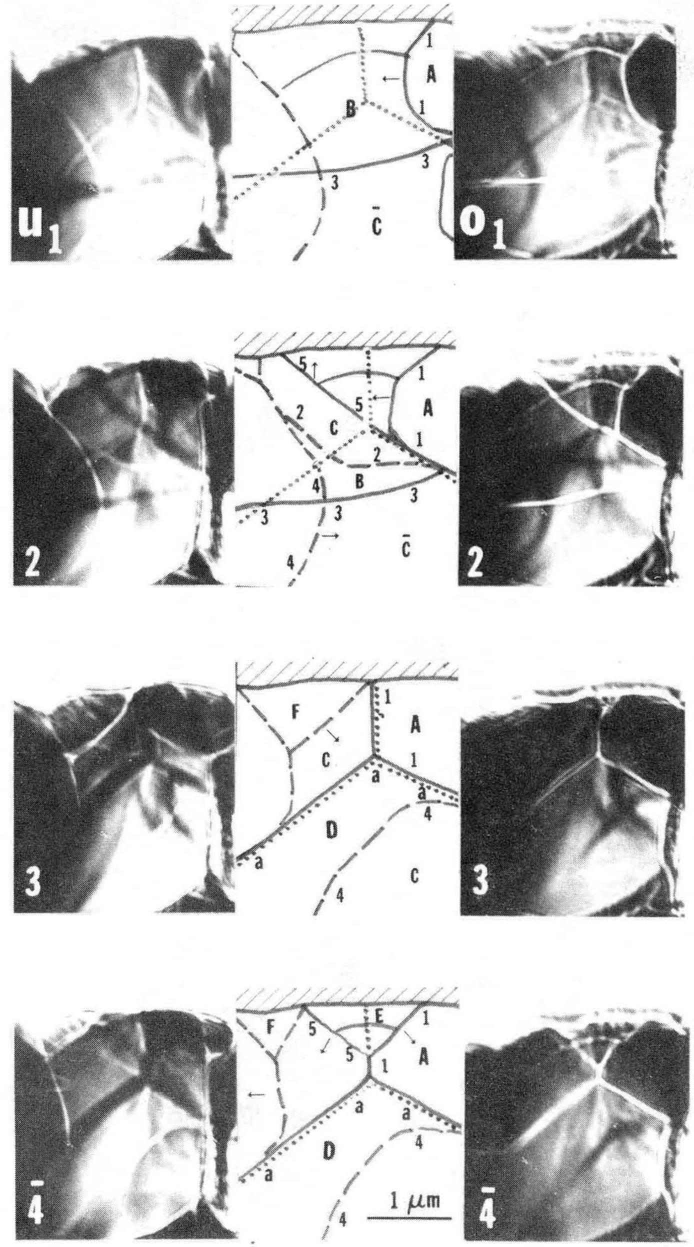

XBB 8010-11966

Fig. 4

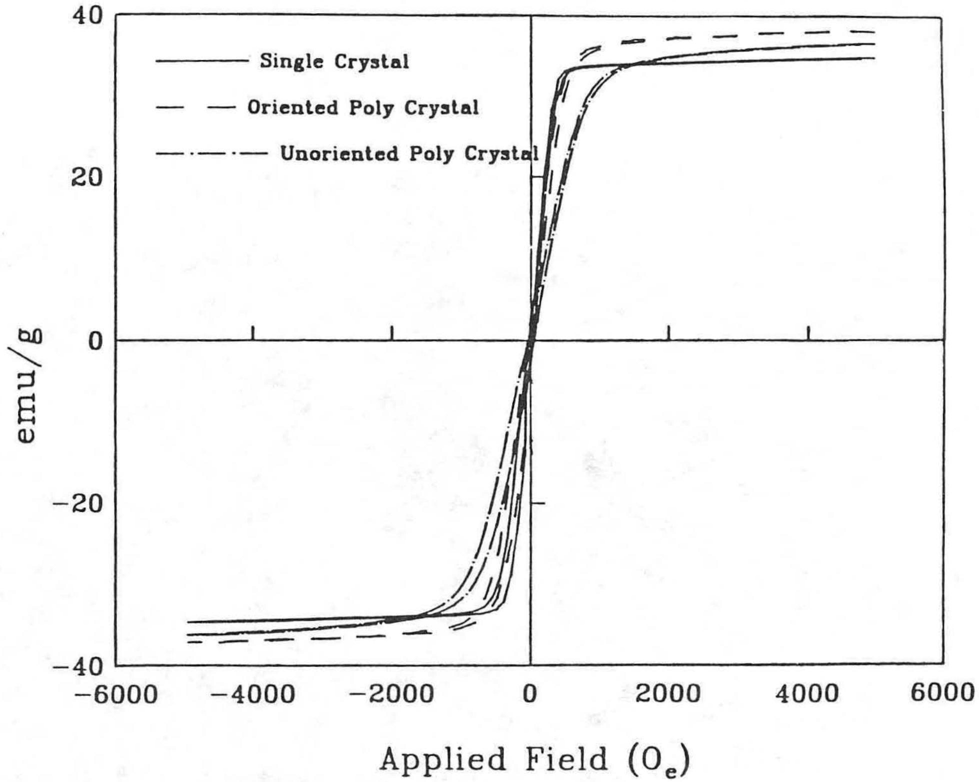

XBL 888-2707

Fig. 5

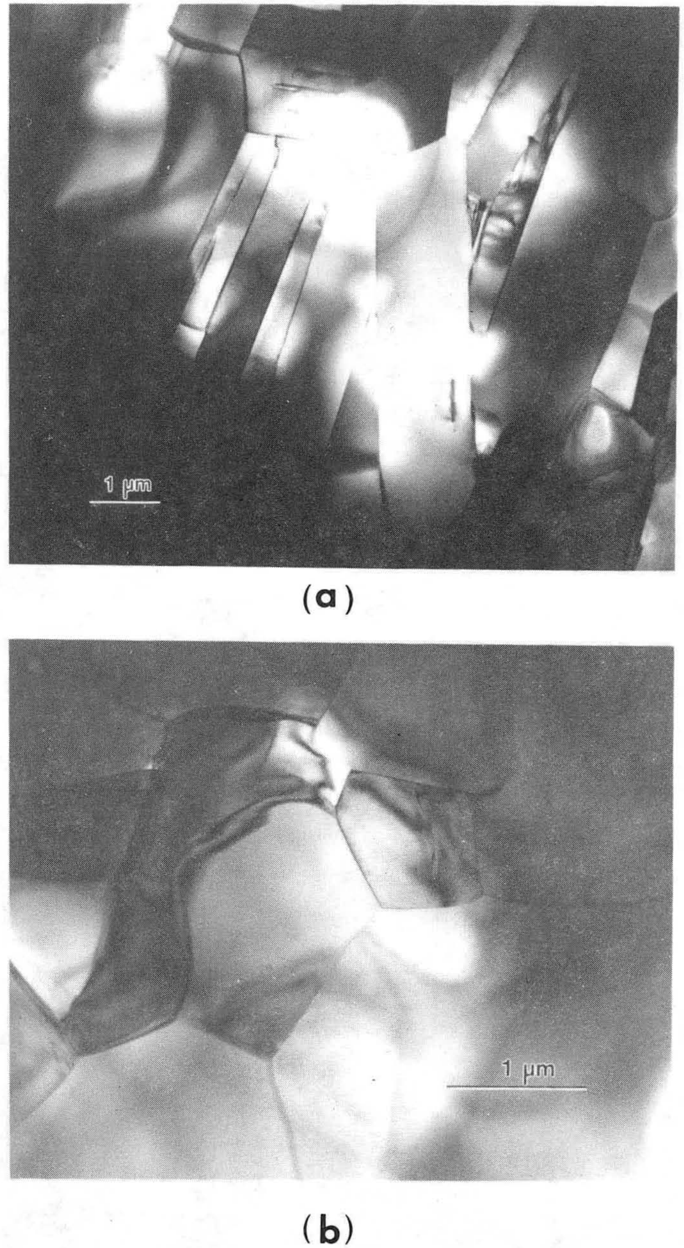

XBB 885-5358A

Fig. 6

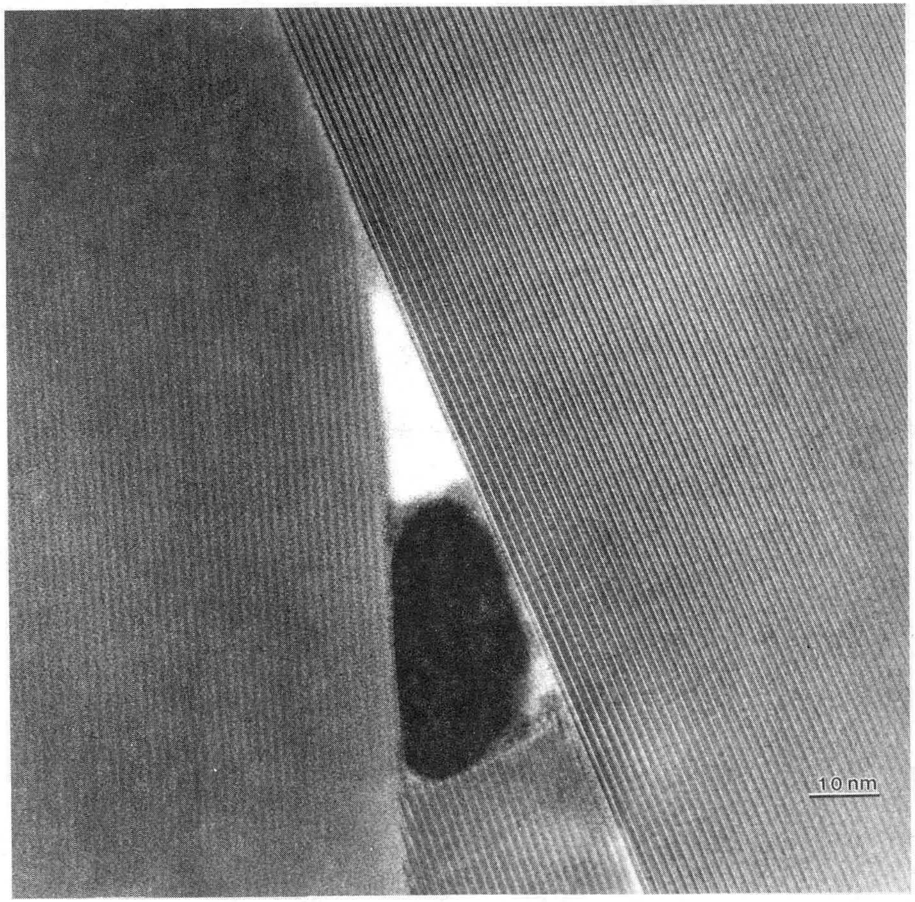

XBB 888-7956

Fig. 7

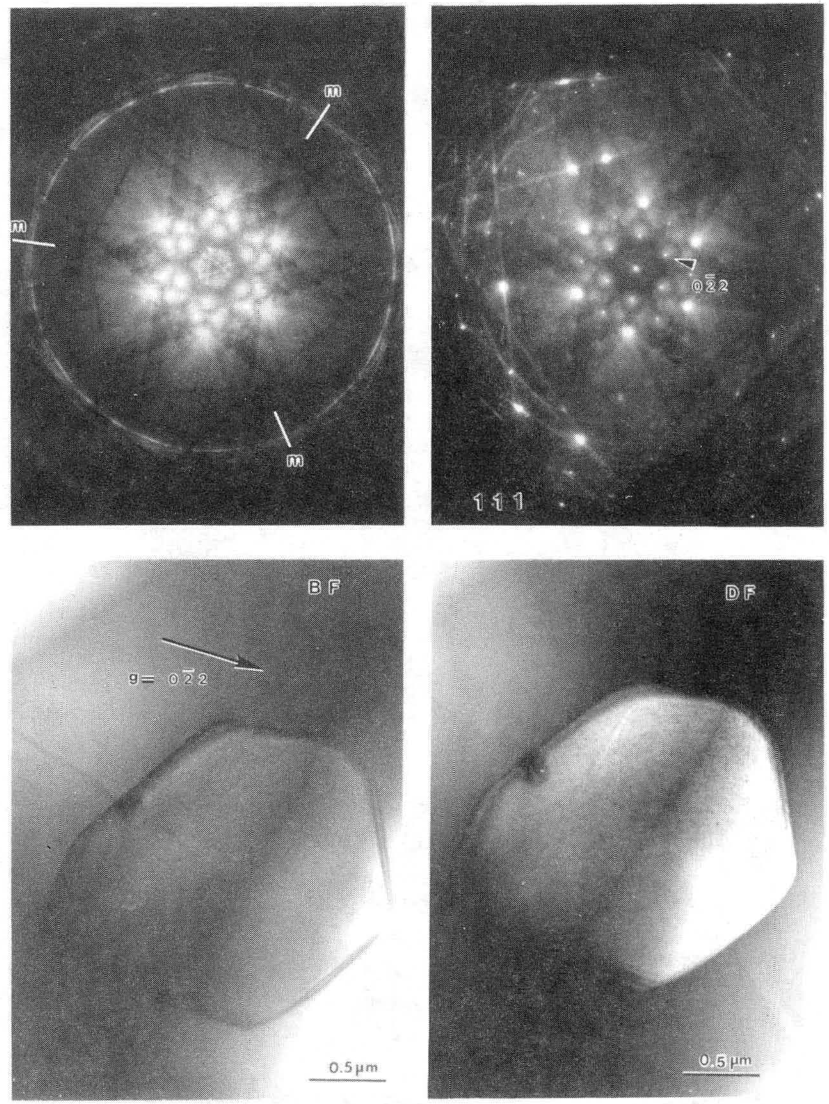

XBB 8711-9542A

Fig.8

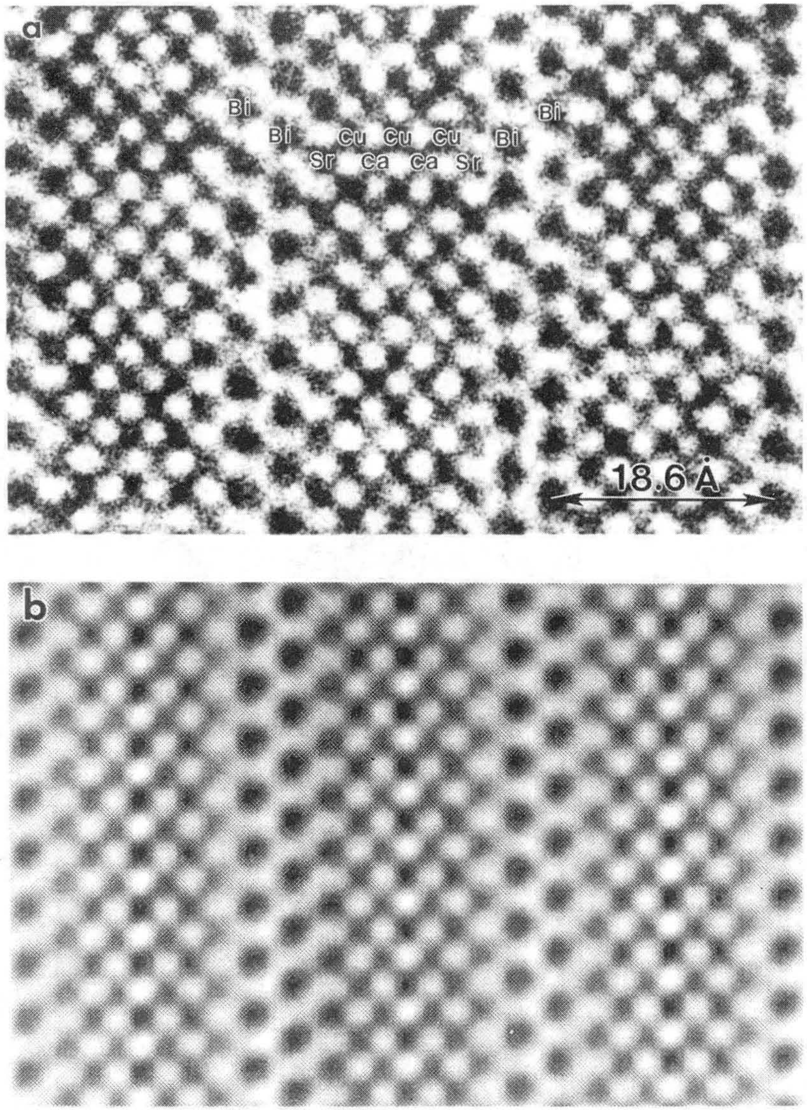

$Bi_2Sr_2Ca_2Cu_3O_y$ (2-2-2-3) T_c = 110K c=37.2Å

XBB 885-4984A

Fig. 9

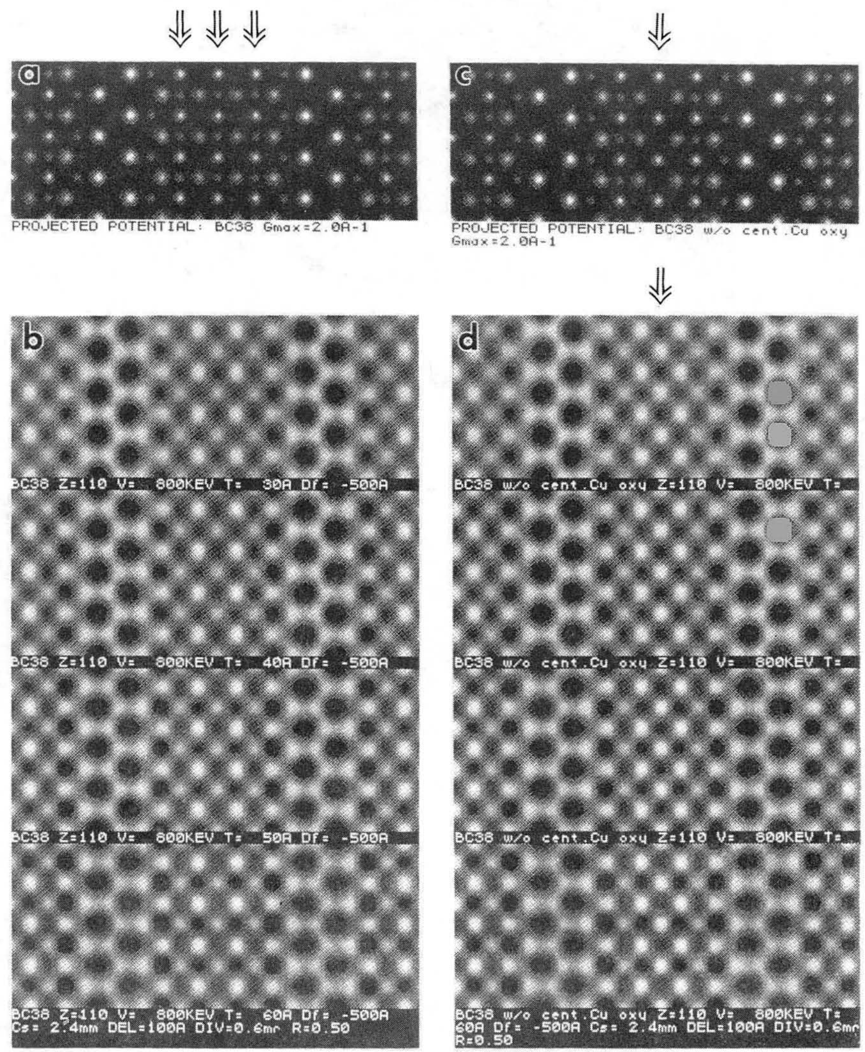

XBB 885-4983

Fig. 10

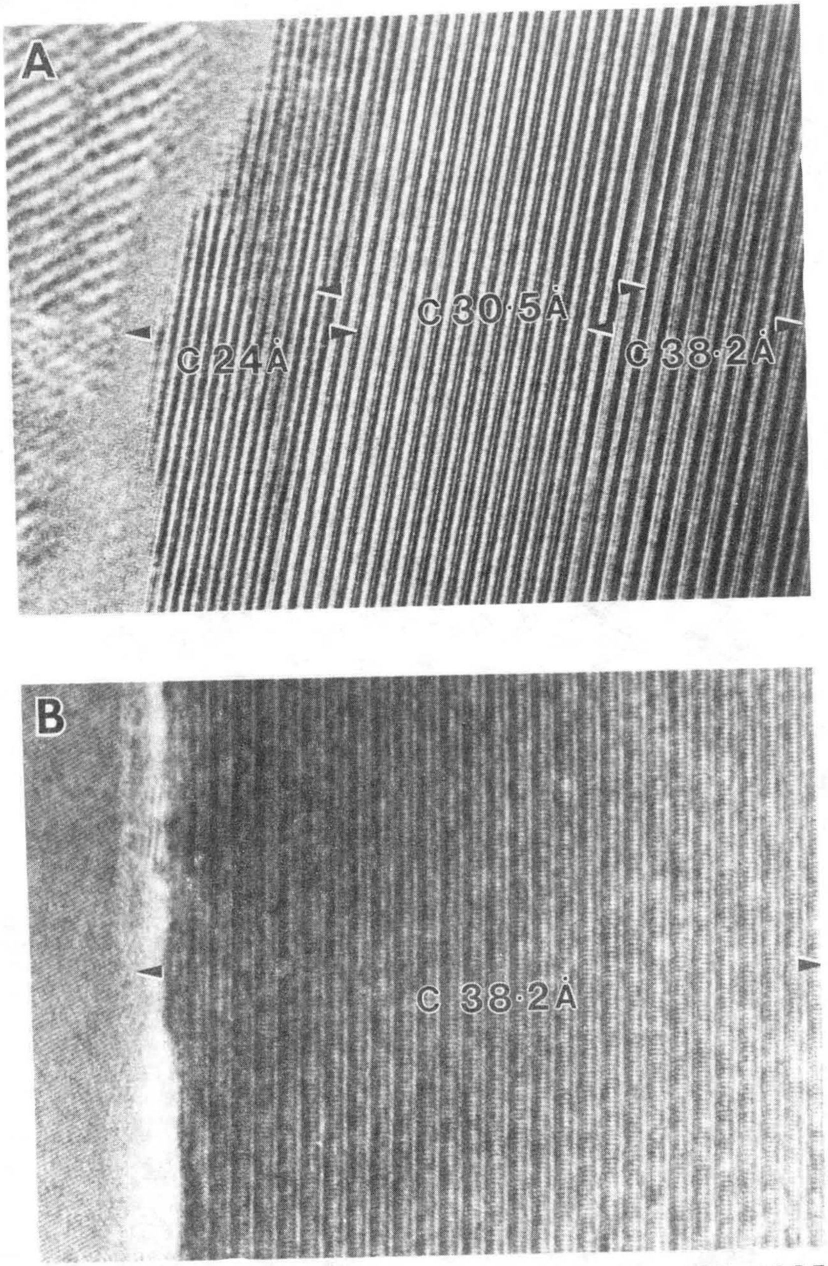

XBB 885-4987

Fig. 11

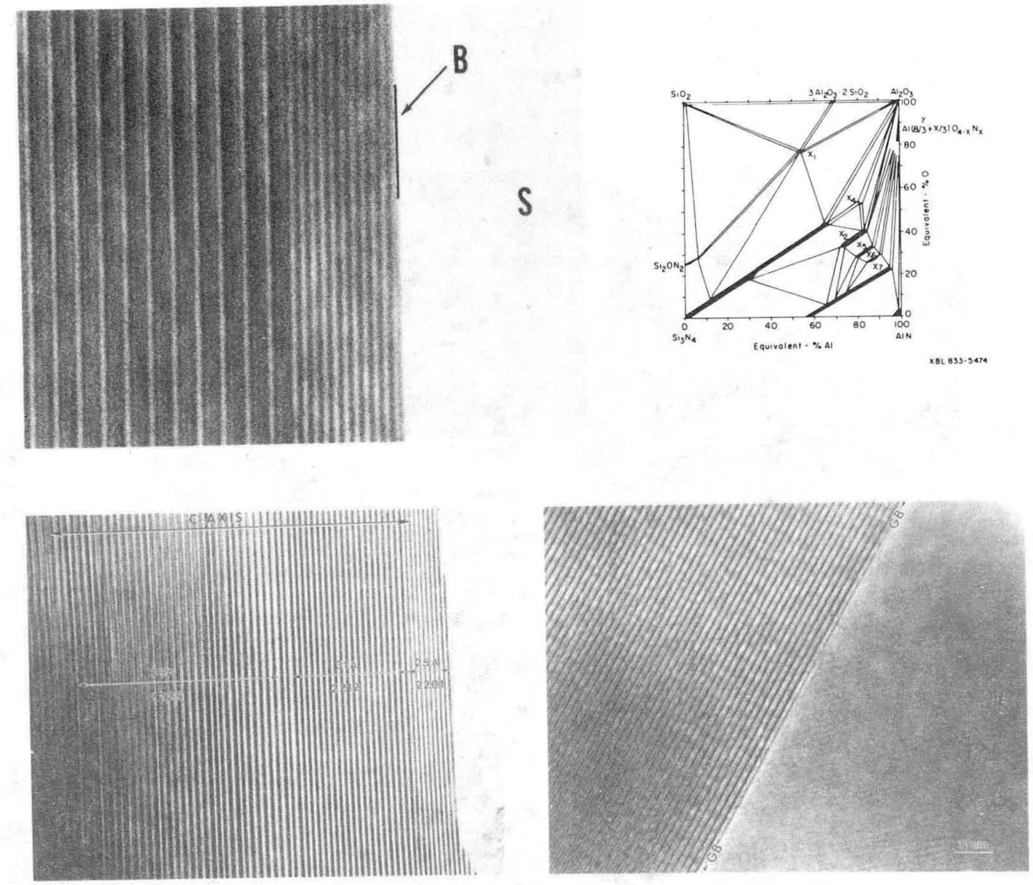

XBB 889-8746

Fig. 12

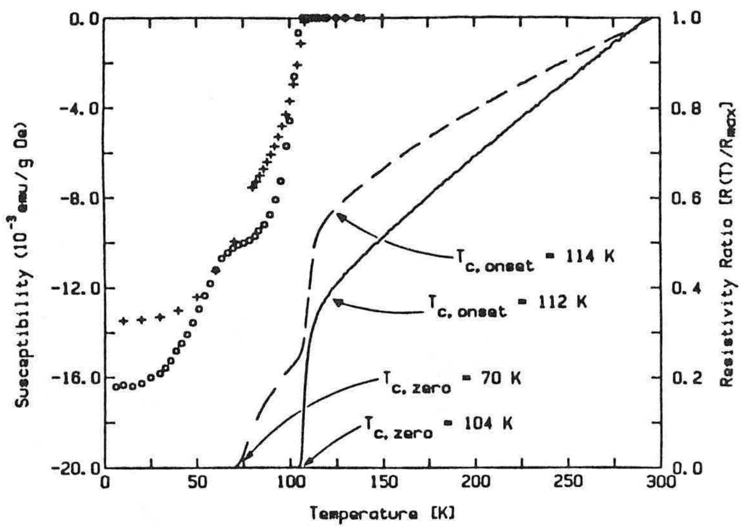

XBL 885-1549

Fig. 13

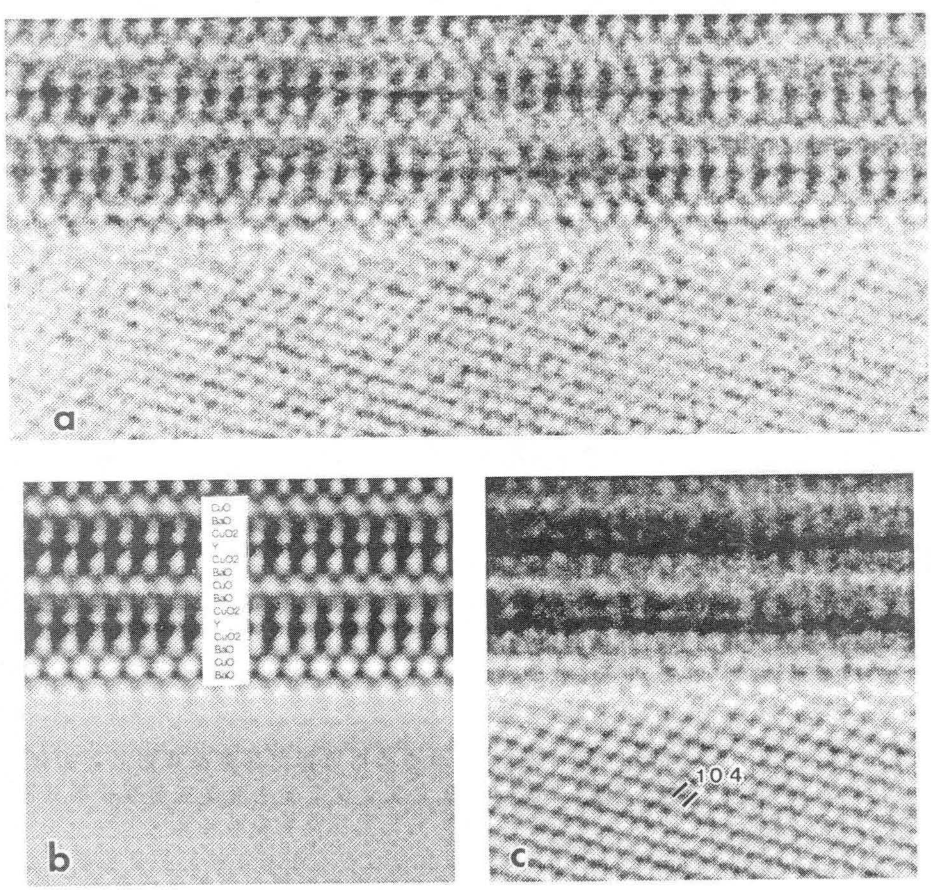

XBB 891-60

Fig. 14